Excited electron-bubble states in superfluid ^{4}He: A time-dependent density functional approach

David Mateo,[1] Dafei Jin,[2] Manuel Barranco,[1] and Martí Pi[1]
[1]*Departament ECM, Facultat de Física, and IN^{2}UB, Universitat de Barcelona. Diagonal 647, 08028 Barcelona, Spain*
[2]*Department of Physics, Brown University, Providence, Rhode Island 02912, USA*

(Received 3 November 2010; accepted 30 December 2010; published online 24 January 2011)

We present a systematic study on the excited electron-bubble states in superfluid ^{4}He using a time-dependent density functional approach. For the evolution of the 1P bubble state, two different functionals accompanied with two different time-development schemes are used, namely an accurate finite-range functional for helium with an adiabatic approximation for electron versus an efficient zero-range functional for helium with a real-time evolution for electron. We make a detailed comparison between the quantitative results obtained from the two methods, which allow us to employ with confidence the optimal method for suitable problems. Based on this knowledge, we use the finite-range functional to calculate the time-resolved absorption spectrum of the 1P bubble, which in principle can be experimentally determined, and we use the zero-range functional to real-time evolve the 2P bubble for several hundreds of picoseconds, which is theoretically interesting due to the break down of adiabaticity for this state. Our results discard the physical realization of relaxed, metastable configurations above the 1P state. © *2011 American Institute of Physics*. [doi:10.1063/1.3544216]

I. INTRODUCTION

Electron bubble (e-bubble) in liquid helium has been an attractive topic for numerous experimental and theoretical studies in the past, and it has drawn again some interest in recent years.[1–11] Density functional (DF) theory has proved to be a powerful tool in dealing with many interesting physical situations involving electron bubbles. When it is applied to optically excited e-bubbles, not only can it achieve quantitative agreement with experiments on the absorption spectra,[1,3,12,13] but it can also nicely display the dynamical evolutions on the picosecond time scale, such as how the bubbles change shapes, release energy, or even break into smaller bubbles.[14,15] These latest works likely require using different density functionals (finite-range or zero-range for liquid helium) in different time-development schemes (adiabatic or real-time evolutions for electron). Regardless of the technical details, the time-dependent density functional approach is no doubt the only workable approach at present for studying the evolution of the excited e-bubble states in liquid helium. The quantitative results drawn from these simulations can be useful to interpret the experimental results and predict new ones.

Upon dipole excitation from the 1S ground state to the 1P or 2P excited state, an e-bubble evolves by relaxing its shape around the excited electron probability density. This relaxation eventually drives the e-bubble back to the spherical 1S ground state. It has been quantitatively shown[15] that depending on the pressure (P) applied to the liquid, this may happen in two different ways. At a pressure below about 1 bar, the e-bubble undergoes damped oscillations for a period of time long enough to allow the electron to radiatively decay to the deformed 1S state, which then evolves radiationlessly to the spherical 1S state. In contrast, at 1 bar or above, the excited e-bubble evolves toward a configuration made of two baby bubbles, so that the probability of finding the electron evenly distributes between them. This two-bubble configuration is unstable against asymmetric perturbations, and one expects this instability to cause the electron to localize in one of the baby bubbles while the other collapses.[12,15,16]

When doing this calculation, the authors of Ref. 15 naturally chose the so-called Orsay–Trento DF.[17] This functional is finite range and incorporates a term that mimics backflow effects in order to accurately reproduce the dispersion relation of the elementary excitations of superfluid ^{4}He. This is instrumental to properly describe the energy transfer from the bubble to the liquid that proceeds by causing all sorts of possible excitations in the superfluid. The token one has to pay for its use is the very high computational cost. Due to the large difference between the intrinsic time scales of electron and helium, this functional is not well adapted for fully real-time, three-dimensional evolutions. Considering this limitation, the adiabatic approximation was used to update the electron wavefunction at every instantaneous helium configuration.[15] One of the main concerns is then to establish how long the adiabatic approximation is valid for. A careful analysis led to the conclusion that it holds for the 1P e-bubble for at least several tens of picoseconds,[15] a period of time large enough to guarantee the reliability of the results obtained for this state. Contrarily, the adiabatic approximation breaks down very quickly for the 2P e-bubble, implying that the existence of relaxed quasiequilibrium 2P bubbles is questionable.

The authors of Ref. 14 followed a different path. Instead of using a finite-range DF, they employed a much simpler zero-range one. This allowed them to carry out fully real-time calculations for hundreds of picoseconds without imposing any adiabatic assumption, at the price of an inaccurate description of the elementary excitations of the liquid. Although this may not qualitatively affect the physical

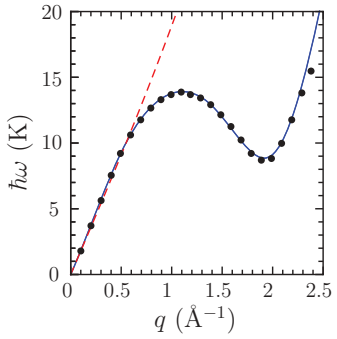

FIG. 1. Dispersion relation of the elementary excitation in bulk liquid ^{4}He at $T = 0$. Solid line: the OT finite-range functional results. Dashed line: the ST zero-range functional results. Dots: the experimental data from Ref. 22.

results, it is unclear how quantitatively reliable are the results so obtained.

In this work, we perform a more systematic study on the relaxation of the excited e-bubbles. We first carry out a detailed comparison between the finite-range and zero-range functionals applied to the 1P bubble problem, through which we gain some insight about their strong points and shortcomings. We then use the finite-range functional to calculate the time-resolved absorption spectrum of the 1P bubble, which can in principle be measured in the experiments. Next, we use the zero-range functional to real-time evolve the 2P bubble for several hundreds of picoseconds, which is of theoretical interest as one can clearly trace how the adiabatic approximation breaks down for this state. These investigations generalize and complement those presented in Ref. 15 within the adiabatic approximation.

Our paper is organized as follows. In Sec. II, we introduce the theoretical framework and numerical schemes. In Sec. III, we discuss the results so obtained. Finally, a summary is presented in Sec. IV. Several movies showing the dynamical evolution of electron bubbles can be found in the supplementary material.[18]

II. THEORETICAL FRAMEWORK

Within the DF approach, the energy of an electron–helium system at zero temperature can be written as a functional of the single-electron wavefunction Φ and the macroscopic helium wavefunction Ψ

$$E[\Phi,\Psi] = \frac{\hbar^2}{2m_e}\int d\boldsymbol{r}\,|\nabla\Phi|^2 + \frac{\hbar^2}{2m_{He}}\int d\boldsymbol{r}\,|\nabla\Psi|^2 + \int d\boldsymbol{r}\,|\Phi|^2\,V_{e-He}[\rho] + \int d\boldsymbol{r}\,\mathcal{E}_{He-He}[\rho]. \quad (1)$$

Specifically, $\Psi = \sqrt{\rho}\exp[\imath S]$ gives the helium particle density ρ and the superfluid velocity $\mathbf{v} = \hbar\nabla S/m_{He}$.[15] $V_{e-He}[\rho]$ is the electron–helium interaction potential,[19] and $\mathcal{E}_{He-He}[\rho]$ is the helium–helium potential energy density. For the sake of comparison, we choose for $\mathcal{E}_{He-He}[\rho]$ either the finite-range Orsay–Trento (OT) density functional,[17] or the zero-range Stringari–Treiner (ST) density functional.[20] It is known that the former one provides a very accurate description of superfluid ^{4}He, particularly of the dispersion relation that covers all the roton excitations up to the wave number $q = 2.3$ Å^{-1}. In contrast, the latter one only reproduces the long-wavelength phonon excitations and is not so accurate, but it has the advantage of high computational efficiency in dynamic evolutions. The dispersion relations obtained from both functionals using the method of Ref. 21 are plotted in Fig. 1 together with the experimental results.[22]

Functional variations of the associated grand potential with respect to Ψ and Φ yield the following Euler–Lagrange equation for the helium and Schrödinger equation for the electron:

$$-\frac{\hbar^2}{2m_{He}}\Delta\Psi + \left\{\frac{\delta\mathcal{E}_{He-He}[\rho]}{\delta\rho} + |\Phi|^2\,\frac{\delta V_{e-He}[\rho]}{\delta\rho}\right\}\Psi = \mu\Psi \quad (2)$$

$$-\frac{\hbar^2}{2m_e}\Delta\Phi + V_{e-He}[\rho]\Phi = \varepsilon\Phi\ , \quad (3)$$

where μ is the helium chemical potential and ε is the electron eigenenergy. Throughout this paper, we treat pressure as a given external condition. The associated chemical potential and particle density in bulk liquid are obtained from the equation of state derived from the DF being used.

The above equations are solved numerically with 13-point finite-difference formulae. In the finite-range DF case, we work in three-dimensional Cartesian coordinates that allow for an extensive use of fast Fourier transformation techniques[23] as explained in Ref. 5. Whenever necessary, we implement a Gram–Schmidt scheme to determine from Eq. (3) the electron spectrum in the helium cavity. In the zero-range DF case, we work in cylindrical coordinates assuming azimuthal symmetry around the z-axis ($r = 0$) and specular symmetry about the $z = 0$ plane. Hence, we only need to solve the equations in the $r \geq 0$ and $z \geq 0$ "quadrant," which greatly speeds up the calculation and so we can attain longer-time physics. There is no difficulty to relax these symmetry restrictions except slowing down the calculation. However, the results are not expected to be very different since there is no detectable symmetry-breaking instability in our problems. For both functionals we use a fairly large spatial step of about 1 Å, without any apparent loss of numerical accuracy.[15]

The time evolution starts from an excited e-bubble state, which means that the electron has been suddenly brought from the 1S onto the 1P or 2P state of the original spherical e-bubble. From this initial configuration, the superfluid helium then evolves according to

$$\frac{\partial\Psi}{\partial t} = -\frac{\imath}{\hbar}\left\{-\frac{\hbar^2}{2m_{He}}\Delta - \mu + \mathcal{U}_{He-He}[\rho,\mathbf{v}] + |\Phi|^2\,\frac{\delta V_{e-He}[\rho]}{\delta\rho}\right\}\Psi, \quad (4)$$

where the detailed form of the effective potential $\mathcal{U}_{He-He}[\rho,\mathbf{v}]$ can be found, e.g., in Refs. 24 and 25.

In the adiabatic approximation scheme, we do not evolve the electron in real-time but keep tracing the instantaneous eigenstates satisfying Eq. (3). In most cases, e-bubbles around excited electron states evolve toward configurations that are

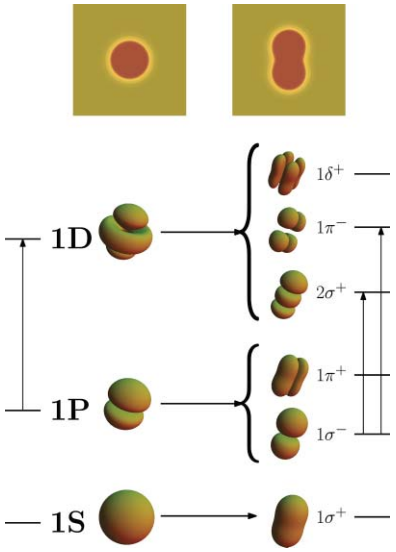

FIG. 2. Splitting of electronic levels along with a representation of their probability densities once the spherical symmetry is broken. The states in the spherical configuration (left) are labeled in the standard nL way. In the axially symmetric case (right) the label is nl_z^s, where $s = +(-)$ stands for symmetric (antisymmetric) states under specular reflection.

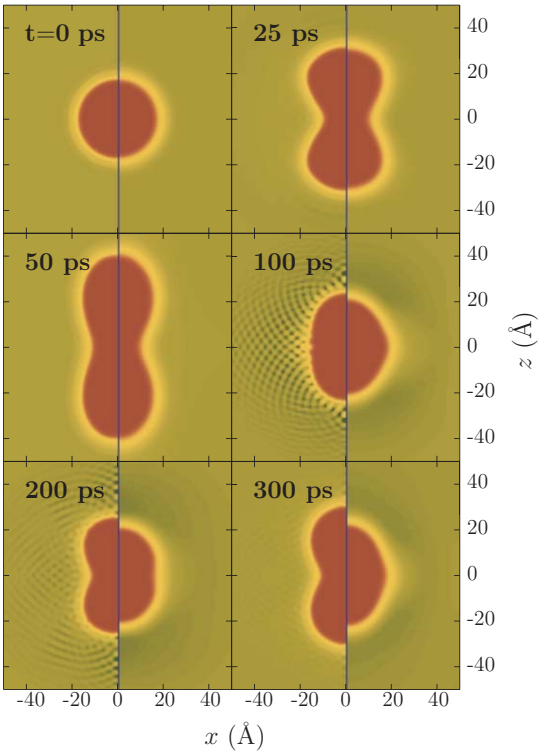

FIG. 3. Evolution of the 1P e-bubble at $P = 0$ bar. The left-hand side of each panel shows the results for the OT finite-range density functional plus adiabatic approximation for the electron. The right-hand side part of each panel shows the results for the ST zero-range density functional plus real-time evolution for the electron.

not spherically but axially symmetric. The originally degenerate angular momentum electron eigenstates in the spherical bubble now split according to the projection (m-values) on the symmetry z-axis, among which only the $\pm m$ states are still degenerate with each other. It is thus convenient to use the notation for the orbital angular momentum of single particle states in linear molecules, i.e., $\sigma, \pi, \delta, \phi, \ldots$ for $|m| = 0, 1, 2, 3, \ldots$ In addition to the axial symmetry, a nP bubble also keeps the original specular symmetry in the course of its evolution. Hence, one can construct the electron eigenbasis in such a way that the electron wavefunctions satisfy $\Phi(r, z, \theta) = \pm\Phi(r, -z, \theta)$. The correspondence between the lower lying spherically and axially symmetric electron states is displayed in Fig. 2 along with a representation of their probability densities. The superscript $+(-)$ denotes specularly symmetric (antisymmetric) states.

In the real-time dynamics scheme, the electron evolves according to

$$\frac{\partial \Phi}{\partial t} = -\frac{\imath}{\hbar}\left\{-\frac{\hbar^2}{2m_e}\Delta + V_{e-He}[\rho]\right\}\Phi\,. \tag{5}$$

We employ a fourth-order Runge–Kutta method to obtain the first time steps, and Hamming's method[26] for subsequent steps. A time step of 10^{-2} ps is chosen for the adiabatic scheme, and of 10^{-6} ps for the real-time dynamics scheme. These very different values reflect the mass ratio $m_e/m_{He} \sim 10^{-4}$. This is the reason that makes a dynamical evolution unaffordable when $\mathcal{E}_{He-He}[\rho]$ is finite-range, since updating the mean field is computationally very costly. Note that the original 1P and 2P levels are threefold degenerate, and that any of the substates (or a superposition of them) can be chosen as the initial state of the electron to start the evolution of the e-bubble. This choice influences the subsequent evolution because $|\Phi|^2$ in Eq. (4) depends on it. We have chosen to initially place the 1P (2P) electron in the $1\sigma^-(3\sigma^-)$ eigenstate because, since the m states are ordered in increasing $|m|$ values when the spherical nL manifold splits,[10] the dynamics of a $m \neq 0$ electron state can be destabilized by small fluctuations at an early stage of its evolution.

During the bubble evolution, sound waves released from its surface eventually reach the cell boundary. If no action is taken, they will bounce back spoiling the calculation. A way to handle this problem is to include some source of damping into Eq. (4) governing the fluid evolution, see e.g., Refs. 1,27, and 28. We have opted by making the replacement $\imath \longrightarrow \imath + \Lambda(\boldsymbol{r})$ in Eq. (4). This corresponds to a rotation of time axis in the complex plane by introducing a damping field $\Lambda(\boldsymbol{r})$, which takes the form[29]

$$\Lambda(\boldsymbol{r}) = \Lambda_0\left[1 + \tanh\left(\frac{s - s_0}{a}\right)\right], \quad s \equiv |\boldsymbol{r}|\,. \tag{6}$$

We keep the dimensionless parameter $\Lambda_0 \simeq 1.6$, and set $a = 5$ Å, $s_0 = 60$ Å in the finite-range calculation, and $a = 8$ Å, $s_0 = 90$ Å in the zero-range calculation. The evolution is damping-free [$\Lambda(\boldsymbol{r}) \ll 1$] in a sphere of radius $s < s_0 - 2a$, which is 50 Å in the finite-range case and 70 Å in the zero-range case. From Figs. 3–6 and the supplementary material[18] one can see that this region is large enough for the 1P e-bubble to expand inside a nondampening environment. For the 2P e-bubble evolution, we use a (r, z) calculation box of 150×150 Å^2 and $s_0 = 120$ Å, leaving ~ 100 Å of nondampening space for the bubble to expand.

The above prescription works extremely well, as it efficiently dampens the excitations of the macroscopic

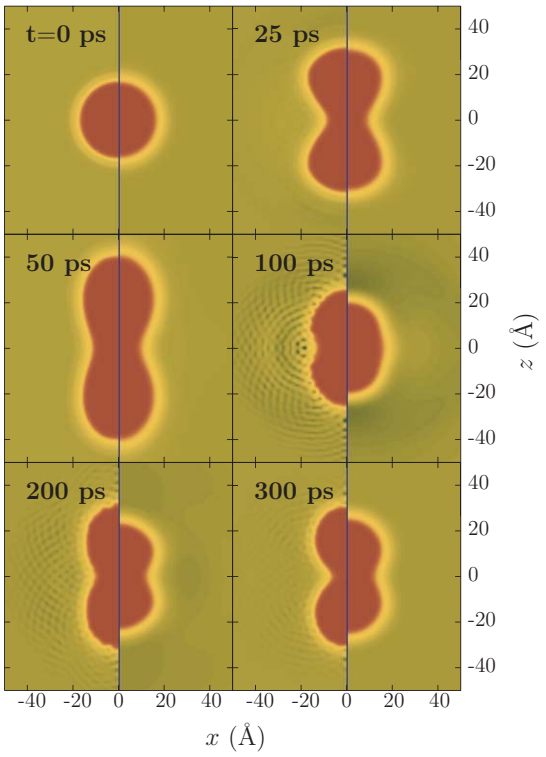

FIG. 4. Same as Fig. 3 at $P = 0.5$ bar.

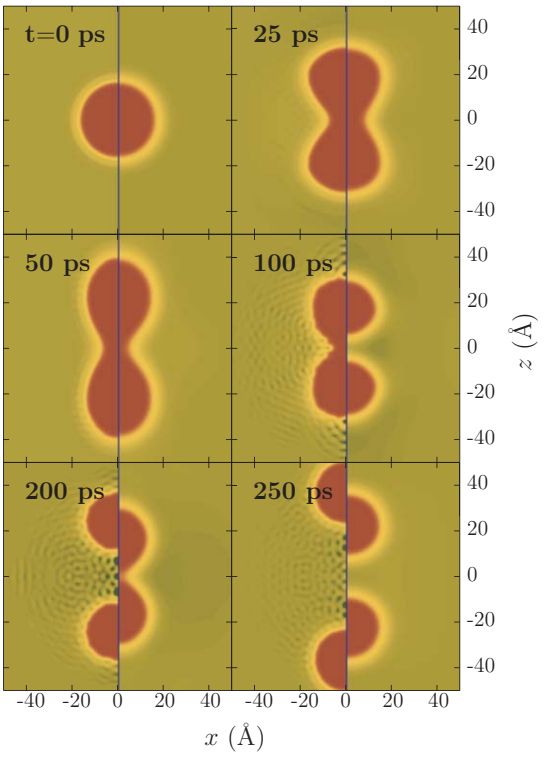

FIG. 5. Same as Fig. 3 at $P = 1$ bar.

wavefunction at the cell boundaries, and does not need a large buffer region to absorb the waves—actually we use the same box where the starting static calculations have been carried out.[14] It allows us to extend the adiabatic calculations of Ref. 15 from tens to hundreds of picoseconds.

III. RESULTS AND DISCUSSION

A. 1P e-bubble dynamics

1. Adiabatic versus real-time dynamical evolution

To some extent, an e-bubble in liquid helium is nearly a textbook example of an electron confined in a spherical-square-well potential. Its static properties are fairly insensitive to the complexities of the chosen functional provided the bulk and surface properties can be well reproduced.[12,13] In particular, a zero-range DF description of the 1S–1P absorption energies of the e-bubble as a function of P does not differ much from that obtained by a finite-range DF description.[3] This means that in some situations one may simply use a zero-range functional, which has an advantage of high computational speed.

Clearly, the dynamics of an e-bubble is much more involved than its statics. In our problems, the—nonspherical—squeezing and stretching of the bubble may cause its waist to shrink to a point when electron tunneling plays a role, and may also dissipate a large amount of energy by exciting elementary modes in the surrounding liquid. So, even if the static properties of the e-bubble are equally well described by both functionals, it is not obvious whether they yield a similar dynamical evolution for an excited e-bubble. This is the first issue we want to address.

We use two different schemes to compute the relaxation of a 1P e-bubble at $P = 0, 0.5, 1$, and 5 bars, and compare the results so obtained. One such scheme is the finite-range OT density functional description for helium with the adiabatic evolution for electron. The other scheme is the zero-range ST density functional description for helium with real-time evolution for the electron.

As can be seen in Figs. 3–6, the evolution starts with the bubble stretching along the z-axis and shrinking on its waist. After this stage, the bubble may continue oscillating and releasing energy into the liquid, eventually reaching a relaxed, metastable 1P state, or may split into two baby bubbles due to the liquid filling-in around the bubble waist. The density waves radiated to the liquid during this evolution take away a considerable part of the energy injected into the system during the absorption process, i.e., 105 meV at $P = 0$ and 148 meV at 5 bar.[3]

In Figs. 3–6 we compare the bubble evolution obtained within the two frameworks for different pressures. At a first glance, both dynamics are nearly equivalent during the first 50 ps, starting to differ from this time on although they are still qualitatively similar. A more detailed analysis, focused on three key elements of the density profiles, indicates the following:

(a). The shape of the bubble surface, defined as the locus where the liquid density equals half the saturation density value ρ_0, e.g., 0.0218 Å^{-3} at $P = 0$ bar. This shape determines the most crucial properties of an e-bubble. From this shape, we know whether the bubble is simply connected or has split. Up to $t \lesssim 50$ ps, the shape of the bubble is nearly identical in both descriptions. At later times, the bubble shape changes at a slower pace in the ST than in the OT description.

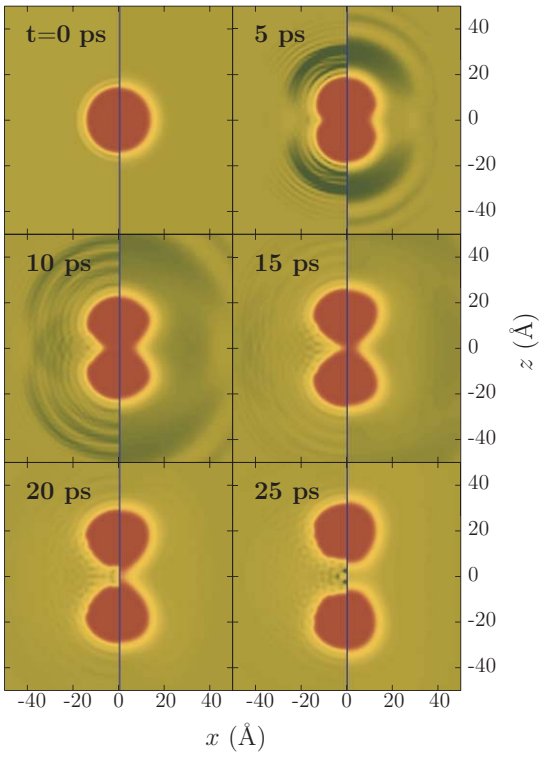

FIG. 6. Same as Fig. 3 at $P = 5$ bar.

Figure 7 illustrates the time evolution of the bubble surface. In particular, the top panel shows the evolution of the point on the bubble surface at $r = 0$ with $z > 0$. This represents half the longitudinal extent of the e-bubble. One can see that this length oscillates in the ST calculation with a lower frequency than in the OT one. Notice that superfluidity is instrumental to keep the bubble surface oscillating without appreciable dampening (yet some energy is still released to the liquid). If helium were in the normal state, these oscillations would be washed out more quickly due to viscosity effects, likely raising the pressure threshold at which the bubble splits.

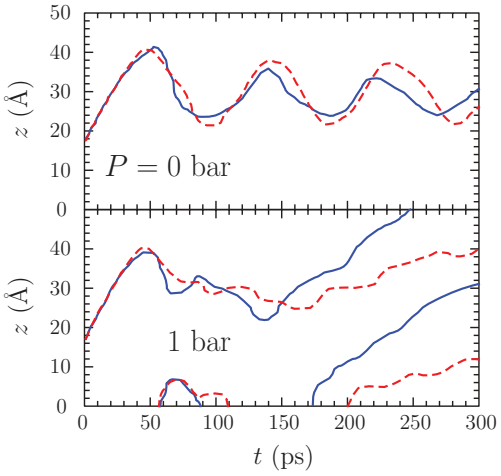

FIG. 7. Evolution of the extent of the bubble along the z-axis at $P = 0$ and 1 bar. The solid line is the OT finite-range result, and the dashed line is the ST zero-range result.

If the bubble symmetrically splits into two baby bubbles, there are two such points, as can be seen in the bottom panel for $P = 1$ bar. We have found that, besides the moment at which the distance between the baby bubbles increases steadily—about 175 ps for the OT functional and 200 ps for ST functional—there is a time interval between ~60 and ~90 ps for the OT functional, and ~60 and ~110 for the ST functional, where the 1P bubble at $P = 1$ bar has split but the emerging baby bubbles are "locked" by the shared electron that exerts some attractive force on them, forcing them back to a simply connected configuration. Eventually, the baby bubbles are unlocked and the distance between them grows.

(b). The surface thickness of the bubble, defined as the width of the region satisfying $0.1\rho_0 \leq \rho(\boldsymbol{r}) \leq 0.9\rho_0$. The thickness of the bubble surface has been found to be nearly independent of the local surface curvature at anytime during the evolution, see also Ref. 15. It is about 1 Å larger in the ST than in the OT description,[17,30] as can be seen in Figs. 3–6 (the blurrier the bubble–helium interface, the larger the surface thickness). The zero temperature OT result, about 6 Å, is in agreement with the experimental findings.[31,32]

(c). The density oscillations traveling through the liquid. This is the point at which the differences between the two functionals become more apparent. The density waves produced by the ST functional have much larger wavelengths because this approach cannot sustain short wavelength inhomogeneities due to the huge energy cost from the $|\nabla\rho(\boldsymbol{r})|^2$ surface energy term. The OT functional has not such a term and is free from this drawback. Roughly speaking, the short wavelength waves arising in the OT approach are smeared out in a sort of big *tsunami* in the ST case, see for instance the panels corresponding to $t = 5$ and 10 ps in Fig. 6. It is worth emphasizing that the wave interference pattern found in the OT description is not an artifact produced by waves bouncing back from the box boundaries, as those are already washed out by the damping term. It arises from the interference of waves produced at different points on the e-bubble surface.

We estimated in Ref. 15 that the first wave front was moving at supersonic velocities, about 330 m/s at $P = 0$ and 410 m/s at $P = 5$ bar. This rises the interesting question of whether shock waves[33] are generated by the displacement of the surface of the bubble. As a matter of fact, a shock wave was launched in the spherical expansion of a highly compressed electron bubble.[1] This wave travelled at supersonic velocities (560 m/s), while the subsequent fronts moved at the speed of sound, some 240 m/s. The analysis carried out by these authors was facilitated by the spherical geometry of the expansion that allowed them to use a very large box for this one-dimensional problem. In our case, the problem is three-dimensional, the wave fronts have a more complex structure and our numerical scheme does not allow to confirm nor discard the appearance of shock waves in the superfluid. In particular, it does not allow us to distinguish between a very distorted density profile, like that we have shown in Fig. 6 of Ref. 15, and a discontinuity in the density and pressure profile characterizing shock waves.[33] Since there is no reason to believe that geometry plays any fundamental role, we are prone to suggest that when the energy released to the liquid is large

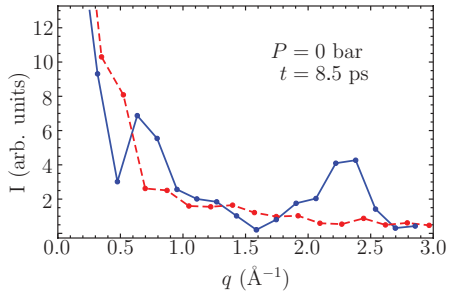

FIG. 8. Fourier transform of the density fluctuation along the z-axis within the region 30 Å $\leq z \leq$ 70 Å for the expansion process of the 1P e-bubble at $P = 0$ bar and $t = 8.5$ ps. The solid line corresponds to the OT calculation, and the dashed line corresponds to the ST functional calculation. The lines have been drawn as a guide to the eye.

enough, as in the 1P to 1S de-excitation at high pressures, or in the 2P to 1S de-excitation, the first launched front is indeed a shock wave.

To quantitatively study the nature of the waves emitted during the bubble evolution, we perform a Fourier analysis of the density profile along the symmetry axis, restricting it to the region 30 Å $\leq z \leq$ 70 Å, away from the bubble location to avoid uncontrolled effects arising from the bubble itself. The Fourier transform of the density fluctuation is shown in Fig. 8 at $t = 8.5$ ps and $P = 0$ bar. While both functionals generate low-q density waves in the phonon region (see Fig. 1) the ST approach does not display any structure, whereas in the OT approach one can identify two distinct peaks. The higher one is located at $q \sim 0.8$ Å^{-1} near the maxon region, and the lower one is located at $q \sim 2.3$ Å^{-1} close to the roton minimum.

With these results on the evolution of the 1P e-bubble in mind, we can state with some confidence that the ST description is accurate enough for describing the fate of the e-bubble, yielding the appropriate final topology at a given pressure, and a more than qualitative picture of its evolution. The shape of the cavity, which is responsible for most electron properties, is essentially the same in both ST and OT descriptions. The different way of energy release associated with their each kind of elementary excitation may yield somewhat diverse evolutions at longer times, but it has little relevance for the problems at hand. One should keep in mind, however, that if the actual subject of the study are the elementary excitations of the bulk liquid, the use of the OT functional is then unavoidable.

We also want to stress that computing the 1P e-bubble dynamics in real time for the ST functional has allowed us to explicitly check the adiabatic approximation in the electron evolution during the time interval relevant for the e-bubble "fission."[15] We have computed the overlap between the time-evolving electron wave function and the instantaneous eigenstate $1\sigma^-$, and have found it to be equal to unity at all times, meaning that the adiabatic approximation holds. As we will discuss later on, this is not the case for the 2P e-bubble.

2. Time-resolved absorption spectrum

Within the OT functional plus adiabatic approximation scheme, we have studied the excitation of 1P bubbles by photoabsorption either to the $m = 0$ component ($2\sigma^+$), or to the $m = \pm 1$ components ($1\pi^-$), arising from the splitting of the originally spherical 1D state, see Fig. 2. In principle, this can be measured in a pump-probe experiment by which the e-bubble is excited by two consecutive laser pulses. The delay set between these pulses corresponds to the time interval between the excitation and the measurement, which is the same as the time defined in our calculations. The intensity of the absorption lines is characterized here by their oscillator strength calculated in the dipole approximation[34]

$$f_{ab} = \frac{2m_e}{3\hbar^2}(E_a - E_b)\left|\langle a|\boldsymbol{r}|b\rangle\right|^2 . \tag{7}$$

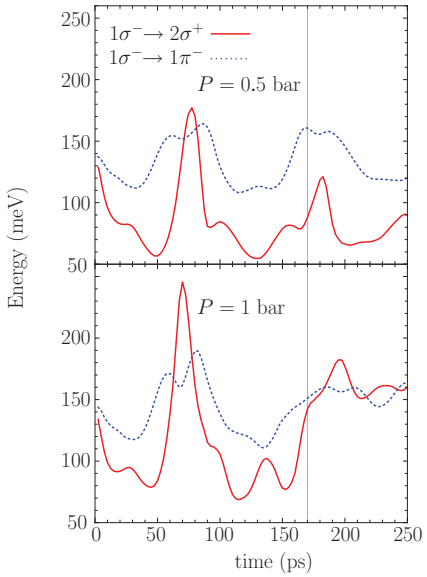

FIG. 9. Time-resolved absorption energies at $P = 0.5$ and 1 bar for the 1P e-bubble evolution. The thin vertical line at $t = 170$ ps indicates the time at which the bubble splits in the $P = 1$ bar case.

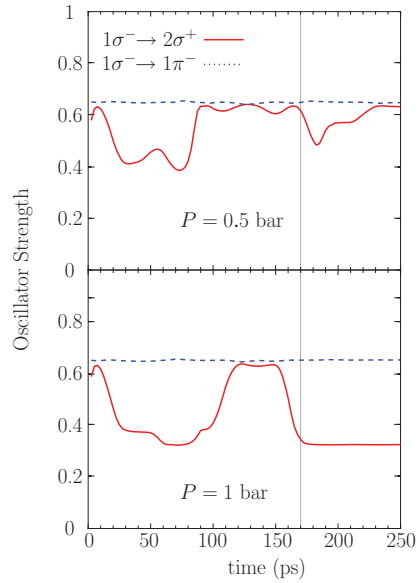

FIG. 10. Time-resolved absorption oscillator strengths at $P = 0.5$ and 1 bar for the 1P e-bubble evolution. The thin vertical line at $t = 170$ ps indicates the time at which the bubble splits at $P = 1$ bar.

We recall that this oscillator strength fulfills the sum rule $\sum_a f_{ab} = 1$, but is generally not positive definite. If the initial state is not the ground state, a partial sum may be greater than unity.

Starting from the 1P electron state $1\sigma^-$ ($m = 0$), the two possible photoexcitation transitions are $1\sigma^- \rightarrow 2\sigma^+$ and $1\sigma^- \rightarrow 1\pi^-$, see Fig. 2. The specularly asymmetric states have a nodal point on the $z = 0$ symmetry plane implying that they are rather insensitive to the presence of helium in that plane. Therefore, the transition energy for excitations between two asymmetric states should not depend much on whether the bubble has split or not. Contrarily, the specularly symmetric states do not have such a nodal point, and so are more sensitive to splitting. The lowest-lying transition connecting specularly asymmetric with specularly symmetric states may thus probe the topology of the bubble, since the absorption energy for this transition should increase by a sizeable amount when the bubble splits. The level structure at the right part of Fig. 2 may help understanding these issues.

The time-resolved absorption energies and oscillator strengths of the evolving 1P bubble for $P = 0.5$ and 1 bar are presented in Figs. 9 and 10. As shown by our calculations, the 1P bubble does not split for $P = 0.5$ bar, but it does for $P = 1$ bar at $t \simeq 170$ ps. The bubble splitting yields a clear signature in the energies and the oscillator strengths: the evolution of the transition energies is similar for $P = 0.5$ and 1 bar before the splitting, but when the bubble splits at $P = 1$ bar, the $1\sigma^- \rightarrow 2\sigma^+$ energy rapidly increases by ~ 70 meV, becoming comparable to the $1\sigma^- \rightarrow 1\pi^-$ energy. This is a consequence of the change in the bubble topology, which makes the final symmetric and antisymmetric states nearly degenerate.

A conspicuous pattern also appears in the evolution of the oscillator strength. The strength for the specularly asymmetric transition $1\sigma^- \rightarrow 1\pi^-$ remains nearly constant at $f \sim 0.65$, whereas the strength for the specularly symmetric transition $1\sigma^- \rightarrow 2\sigma^+$ oscillates when the bubble is simply connected but falls down to $f \sim 0.32$ when the bubble splits. This is again a consequence of the near degeneracy of symmetric and asymmetric states in the split-bubble regime. The oscillator strength for the antisymmetric transition is a factor of 2 larger than that of the symmetric transition in the split-bubble regime because the final state $1\pi^-$ is twofold degenerate.[35]

We thus conclude that time-resolved absorption energies are of practical interest because they bring rich information on the bubble shape and can be determined in experiments. This may shed light on the longstanding question about whether 1P e-bubbles under pressure do really "fission" into two baby bubbles as our calculations indicate, and how the electron wavefunction collapses into one of them, without violating the quantum measurement axiom.

B. 2P e-bubble dynamics: the breakdown of adiabaticity

Our previous analysis of the dynamics of the 1P e-bubble has shown that one does not need to use the accurate OT functional to describe this process. The much simpler ST approach already yields a fair description. This is particularly useful when we move to the study of the 2P e-bubble dynamics. An attempt to simulate this evolution has been made within the OT approach and the adiabatic approximation.[15] This could only be performed for a few picoseconds, as it was shown that the adiabatic approximation fails at $t \simeq 7.4$ ps. This failure is due to the approaching of the $3\sigma^-$ (arising from the spherical 2P level) and $2\sigma^-$ (arising from the spherical 1F level) energy levels. By using the efficient real-time ST scheme, we now relax the adiabatic approximation, following the evolution of the 2P e-bubble for several hundreds of picoseconds. We keep referring to this bubble as a "2P e-bubble," but should have in mind that once the adiabatic approximation breaks down, the electron is no longer in the original eigenstate. Generally, it is in a superposition of states that have the same quantum numbers as the initial state, here meaning that it can be in any superposition of σ^- states.

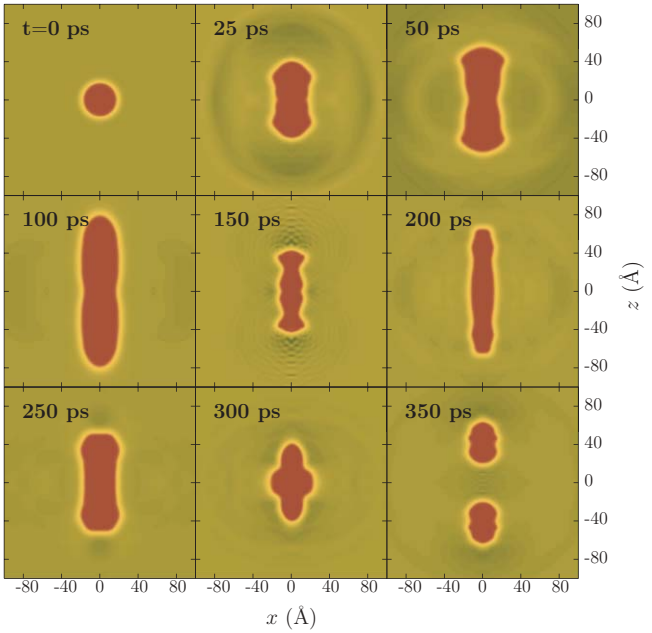

FIG. 11. Evolution of the 2P e-bubble at $P = 0$ bar using real-time dynamics and the ST zero-range functional.

The 2P bubble evolution is shown in Fig. 11. For the first 100 ps, the shape evolution of the 2P bubble is similar to that of the 1P bubble, as it expands along the symmetry z-axis while its waist shrinks in the perpendicular plane. From this point on, the bubble oscillates back and forth in a kind of four-lobe shapes quite different from those seen in the 1P bubble. We attribute these conspicuous shape variations to the breaking down of the adiabatic approximation as the electron moves from a eigenstate to a nontrivial superposition of those compatible with the symmetries of the system. After evolving for ~325 ps, the 2P bubble splits into two baby bubbles.

We present in Fig. 12(a) the evolution of the *instantaneous* eigenenergies of the first σ^- states. As can be seen in panel (b), the $2\sigma^-$ and $3\sigma^-$ states nearly meet at $t \simeq 7.4$ ps. In agreement with some well-known results from basic quantum mechanics,[36] we have found that this situation corresponds to an avoided crossing. Panel (c) shows the overlap of the evolving electron wavefunction with the relevant instantaneous eigenstates. The electron is initially in a $3\sigma^-$ state (the overlap is unity), but at the point of avoided crossing the

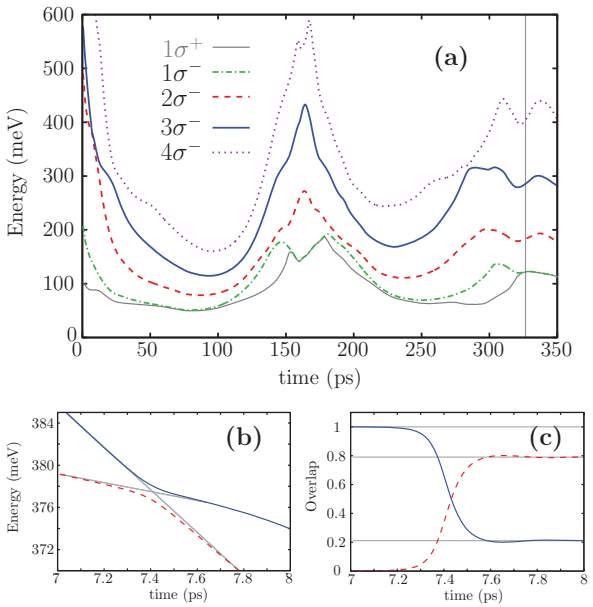

FIG. 12. (a): Lower-lying *instantaneous* σ^- eigenstates together with the $1\sigma^+$ eigenstate of the 2P e-bubble at $P = 0$ bar as a function of time. The thin vertical line at $t = 325$ ps indicates the time at which the bubble splits. (b) Enlarged view of the region where the $3\sigma^-$ and $2\sigma^-$ states repel each other. (c) Overlap of the time-evolving electron state onto the $3\sigma^-$ (solid line) and $2\sigma^-$ eigenstates (dashed line), $|\langle\Phi(\boldsymbol{r}, t)|n\sigma^-\rangle|^2$. The adiabatic approximation fails if the value of this overlap varies in time.

adiabaticity is lost: the electron state is a superposition of the $2\sigma^-$ ($\sim 80\%$) and $3\sigma^-$ ($\sim 20\%$) states.

We have also found a time interval between $\sim$155 and $\sim$180 ps when the 2P bubble at $P = 0$ bar has split but the emerging baby bubbles do not go away. When this happens, the $n\sigma^-$ and $n\sigma^+$ states should be degenerate. This is illustrated in panel (a) of Fig. 12 for the $n = 1$ states. Notice from Fig. 11 that in the $50\,\text{ps} \lesssim t \lesssim 100\,\text{ps}$ interval the bubble is simply connected and the apparent degeneracy displayed in Fig. 12(c) is due to the energy scale. The same thing happens around $t \sim 230$ ps.

IV. SUMMARY

We have thoroughly studied the dynamical evolution of 1P and 2P excited electron bubbles in superfluid ^{4}He at zero temperature. To this end, we have resorted to zero- and finite-range density functionals, establishing how reliable the former is by comparing its results with those obtained with the latter.

Although the results obtained for the 1P bubble evolution from these two functionals show some quantitative differences, especially for long-time evolutions, they are qualitatively equivalent. In particular, both lead to the conclusion that 1P bubbles "fission" at pressures above 1 bar. The ST functional result is of particular relevance, as it has been obtained by a real-time evolution, without assuming the adiabaticity of the process. This confirms the previous results obtained using the finite-range OT functional and the adiabatic approximation for much shorter periods of time than in the present work.[15]

Some indirect experimental evidence indicates a change in the de-excitation behavior of the 1P e-bubble as pressure increases.[12,16] We have explored here the possibilities offered by the photoabsorption spectrum of the 1P e-bubble to disclose whether such a bubble de-excites by "fission" or by a more conventional radiative decay, and have obtained the signatures that would help distinguish between both decay channels. Although far from trivial, a pump-probe experiment may detect a change in the absorption spectrum of the 1P bubble associated with the appearance of the two baby bubble de-excitation channel.

Finally, we have studied the evolution of the 2P e-bubble in real-time within the ST functional approach. We have dynamically found that the adiabatic approximation does not hold at any positive pressure confirming the results obtained within the OT plus adiabatic approximation approach.[15] Negative pressures, as those attained in cavitation experiments, have not been studied. The physical realization of a relaxed, metastable 2P configuration is discarded.

ACKNOWLEDGMENTS

The authors wish to thank Humphrey Maris for helpful discussions. This work was performed under Grant Nos. FIS2008-00421/FIS from DGI, Spain (FEDER), and 2009SGR1289 from Generalitat de Catalunya. D.M. has been supported by the Spanish MEC-MICINN through the FPU fellowship program, Grant No. AP2008-04343. D.J. has been supported by the National Science Foundation of the United States through Grant No. DMR-0605355.

[1] J. Eloranta and V. A. Apkarian, J. Chem. Phys. **117**, 10139 (2002).
[2] A. Ghosh and H. J. Maris, Phys. Rev. Lett. **95**, 265301 (2005).
[3] V. Grau, M. Barranco, R. Mayol, and M. Pi, Phys. Rev. B **73**, 064502 (2006).
[4] M. Rosenblit and J. Jortner, J. Chem. Phys. **124**, 194505 (2006); *ibid.* **124**, 194506 (2006).
[5] M. Pi, R. Mayol, A. Hernando, M. Barranco, and F. Ancilotto, J. Chem. Phys. **126**, 244502 (2007).
[6] L. Lehtovaara and J. Eloranta, J. Low Temp. Phys. **148**, 43 (2007).
[7] H. J. Maris, J. Phys. Soc. Jpn. **77**, 1 (2008).
[8] W. Guo, D. Jin, G. M. Seidel, and H. J. Maris, Phys. Rev. B **79**, 054515 (2009).
[9] F. Ancilotto, M. Barranco, and M. Pi, Phys. Rev. B **80**, 174504 (2009).
[10] D. Mateo, A. Hernando, M. Barranco, and M. Pi, J. Low Temp. Phys. **158**, 397 (2010).
[11] D. Jin and H. J. Maris, J. Low Temp. Phys. **158**, 317 (2010).
[12] C. C. Grimes and G. Adams, Phys. Rev. B **41**, 6366 (1990).
[13] C. C. Grimes and G. Adams, Phys. Rev. B **45**, 2305 (1992).
[14] D. Jin, W. Guo, W. Wei, and H. J. Maris, J. Low Temp. Phys. **158**, 307 (2010).
[15] D. Mateo, M. Pi, and M. Barranco, Phys. Rev. B **81**, 74510 (2010).
[16] H. J. Maris, A. Ghosh, D. Konstantinov, and M. Hirsch, J. Low Temp. Phys. **134**, 227 (2004).
[17] F. Dalfovo, A. Lastri, L. Pricaupenko, S. Stringari, and J. Treiner, Phys. Rev. B **52**, 1193 (1995).
[18] See supplementary material at http://dx.doi.org/10.1063/1.3544216 for movies of the dynamical evolution of electron bubbles.
[19] E. Cheng, M.W. Cole, and M.H. Cohen, Phys. Rev. B **50**, 1136 (1994); Erratum Phys. Rev. B **50**, 16134 (1994).
[20] S. Stringari and J. Treiner, Phys. Rev. B **36**, 16 (1987); J. Chem. Phys. **87**, 5021 (1987).
[21] D. Mateo, J. Navarro, and M. Barranco, Phys. Rev. B **82**, 134529 (2010).
[22] R. J. Donnelly, J. A. Donnelly, and R. N. Hills, J. Low Temp. Phys. **44**, 471 (1981).

[23]M. Frigo and S. G. Johnson, Proc. IEEE **93**, 216 (2005).
[24]L. Giacomazzi, F. Toigo, and F. Ancilotto, Phys. Rev. B **67**, 104501 (2003).
[25]L. Lehtovaara, T. Kiljunen, and J. Eloranta, J. Comput. Phys. **194**, 78 (2004).
[26]A. Ralston and H. S. Wilf, *Mathematical Methods for Digital Computers* (John Wiley and Sons, New York, 1960).
[27]C. Cerjan, D. Kosloff, R. Kosloff, and M. Reshef, Geophysics **50**, 705 (1985).
[28]D. Neuhauser and K. Lopata, J. Chem. Phys. **129**, 134106 (2008).
[29]D. Jin and W. Guo, Phys. Rev. B **82**, 094524 (2010).
[30]J. Dupont-Roc, M. Himbert, N. Pavloff, and J. Treiner, J. Low Temp. Phys. **81**, 31 (1990).
[31]J. Harms, J. P. Toennies, and F. Dalfovo, Phys. Rev. B **58**, 3341 (1998).
[32]K. Penanen, M. Fukuto, R. K. Heilmann, I. F. Silvera, and P. S. Pershan, Phys. Rev. B **62**, 9621 (2000).
[33]L. Landau and E. Lifchitz, *Mécanique des Fluides* (Éditions Mir, Moscow, 1971).
[34]M. Weissbluth, *Atoms and Molecules* (Academic, New York, 1978).
[35]Fig. 10 displays the oscillator strength *per energy level* and not *per state*. π states are twofold degenerate due to the two possible l values, $l = \pm 1$, while σ states are nondegenerate as $l = 0$. For this reason, when these states become nearly degenerate in the split-bubble regime, one transition has $f \sim 0.32$ and the other $f \sim 0.65$, a factor of 2 larger.
[36]E. Teller, J. Phys. Chem. **41**, 1 (1937).